NASA TN D-3957

EFFECTIVE RESONANCE INTEGRALS OF SEPARATED TUNGSTEN ISOTOPES

By Donald F. Shook and Donald Bogart

Lewis Research Center
Cleveland, Ohio

NATIONAL AERONAUTICS AND SPACE ADMINISTRATION

For sale by the Clearinghouse for Federal Scientific and Technical Information
Springfield, Virginia 22151 – CFSTI price $3.00

EFFECTIVE RESONANCE INTEGRALS OF SEPARATED TUNGSTEN ISOTOPES

by Donald F. Shook and Donald Bogart

Lewis Research Center

SUMMARY

Measurements of effective resonance integrals for separated tungsten isotopes enriched in tungsten 182, 183, 184, and 186 and for natural tungsten were made relative to gold. The effective integrals were determined by using a small homogeneous reactor to measure epicadmium reactivities for samples of various sizes located at the center of the core. For comparison with the reactivity data, relative γ-ray activities of cadmium-covered thin samples of gold were also determined.

The experimental results were compared with effective resonance integral calculations by using the Nordheim integral method and recently measured isotopic resonance parameters. Agreement between the calculations and experimental results for tungsten 182, 183, and 184 were generally good. However, for the tungsten 186 samples and for thick samples of natural tungsten, the calculations overestimated experimental effective integrals by 10 to 20 percent. For tungsten 186, the use of a radiation width of 44±4 millivolts for the highly scattering 18.8-electron-volt resonance brought calculations and experiment into better agreement. For natural tungsten, the experimental results indicated the presence of overlap effects for resonances of constituent isotopes.

INTRODUCTION

A reactor design limitation associated with the use of tungsten in high-temperature thermal spectrum reactors is introduced by the relatively large capture cross sections (ref. 1) of natural tungsten for resonance and thermal neutrons. The isotope tungsten 184 has relatively few resonances and a small thermal cross section; thus, tungsten enriched in this isotope is more suitable for thermal reactor application. However, the cross sections for all the tungsten isotopes should be known accurately and a method for calculating capture rates in finite-sized samples should be available in order to evaluate the

neutronic characteristics of proposed reactors containing tungsten enriched in tungsten 184. Therefore, measurements of effective resonance integrals for the small quantities of separated tungsten isotopes available are useful as tests of presently known cross sections and calculational methods.

The calculational problem for tungsten is different than that for uranium 238 for which extensive comparison with experiment has been made in the past. In the case of tungsten, neutron captures below the first resonance account for a large fraction of the total captures, and scattering widths are much larger than capture widths for important resonances. For uranium 238 neither of these effects is present. For highly scattering resonances, the spatially flat source approximation used in computing the neutron escape probability for the sample appears inadequate.

Although the reported parameters of the most prominent isotopic resonances of tungsten have been evaluated (refs. 1 and 2), the precision of these early transmission data can be improved by newer analytical techniques. The more recent transmission data (refs. 3 and 4) and capture data (refs. 5 and 6) for tungsten have identified a large number of additional resonances. Since the scattering widths for some of the resonances are large, it is difficult to derive capture widths from the transmission data. The measured scattering widths must be used to derive capture widths from the capture measurements. An iterative analytic procedure using transmission and capture data should provide more precise resonance parameters as additional data becomes available.

The effective resonance integral I_{eff} for a sample in a neutron slowing-down medium is defined as the lethargy-integrated capture cross section that yields the correct capture rate when the sample is exposed to the unperturbed flux spectrum that would be present in the absence of the sample. For the case of a very thin sample, I_{eff} is the dilute resonance integral and is related to the energy-dependent microscopic capture cross section $\sigma_c(E)$ in the following way:

$$I_{eff} = \int_{E_{Cd}}^{\infty} \sigma_c(E) \frac{dE}{E} \qquad (1)$$

where the slowing-down flux in the surrounding medium is standardized to vary inversely with neutron energy E and E_{Cd} is an effective cadmium-filter cutoff energy.

For a thick sample or lump of material, the flux distribution changes so that I_{eff} depends on a volume integral of the product of the actual flux in the sample and the capture cross section.

$$NV\varphi_o I_{eff} = \int_{E_{Cd}}^{\infty} \int_r N \sigma_c(E) \varphi(E, r) dE \, dr \qquad (2)$$

where N is the sample atom density, V the sample volume, and φ_0 the total unperturbed flux. It is implicit in equation (2) that the flux per unit energy $\varphi(E)$ varies as 1/E when the thick sample is not present; therefore, equation (2) reduces to equation (1) for thin samples.

The upper and lower limits of the energy integrals in equations (1) and (2) represent a standardization of what is to be measured for a cadmium-filtered sample. The value of E_{Cd} used is 0.5 electron volt.

Resonance capture can be calculated with precision for a wide range of sample geometries and temperatures if accurate resonance parameters have been measured. Methods for calculating I_{eff} from resonance parameters and statistical distributions of these parameters are available. Summaries of analytical methods are presented in references 7 and 8. The analytical method used herein is the digital computer technique based on methods presented in reference 8. The technique employs a direct numerical integration of the integral equations representing neutron captures and scattering processes in a sample. The method makes use of the flat-source assumption for computing escape probabilities that accounts for scattering in the sample. This source distribution is a good approximation for resonance-capture calculations in uranium 238. However, this method is applicable to isotopes with widely spaced resonances and may not be sufficiently accurate for the highly scattering or closely spaced resonances that are present in tungsten.

Many of the experimental and analytical methods developed from the large amount of effective resonance integral work that has been done with uranium 238 can be applied to tungsten. However, the activation technique, commonly used for uranium 238, can not be used for tungsten since two of the four most abundant tungsten isotopes are not made radioactive following neutron capture. Consequently, a more difficult reactivity measurement technique was used to measure resonance integrals for separated isotopes of tungsten.

METHOD OF MEASUREMENT

The reactivity $\Delta K/K$ of a cadmium-covered purely absorptive sample located at the center of a reactor is given by perturbation theory in references 9 and 10 as

$$\frac{\Delta K}{K} = \frac{-\int_{E_{Cd}}^{\infty} \int_{r} N\sigma_c(E)\varphi(E,r)\varphi^*(E,r)dE\ dr}{F_{tot}} \tag{3}$$

where $\varphi^*(E,r)$ is the unperturbed adjoint function at the sample and F_{tot} is the integrated total fission rate in the reactor. The remaining notation in expression (3) is the same as for expression (2).

In a thermal reactor, $\varphi^*(E)$ is essentially constant and $\varphi(E)$ varies as $1/E$ in the resonance region of interest. Since E_{Cd} is approximately 0.5 electron volt, equation (3) can be rewritten by using equation (2):

$$\frac{\Delta K}{NVK} = - CI_{eff} \tag{4}$$

In equation (4), the constants F_{tot} and φ_o are combined into the constant C, and $\Delta K/NVK$ is the reactivity coefficient for the resonance absorber.

The proportionality expressed by equation (4) permits the reactivity coefficients of unknown resonance absorbers to be related to effective resonance integrals by using an isotope with a known resonance integral as a standard to determine the constant C. The resonance level structures for the samples to be measured are different from that of the standard, so that the proportionality expressed by equation (4) is not exact. However, since the reactor flux and important resonance cross sections are known, a correction can be calculated to make the reactivity coefficients for the samples of interest more precise. These corrections and other reactivity effects that are extraneous to the evaluation of I_{eff} are also accounted for.

The following phenomena in the reactivity measurements were investigated:

(1) Departure of the reactor flux $\varphi(E)$ from a $1/E$ variation

(2) Variation of the adjoint function $\varphi^*(E)$ from constancy

(3) Deviation of the cadmium thermal neutron filter from a sharp filter with a 0.5-electron-volt cutoff energy

(4) Scattering by the sample of neutrons by elastic and inelastic processes. (This introduces a small positive reactivity effect by shifting neutrons at the center of the core from high energy having low importance to lower energy having greater importance.)

The corrections involving the fluxes and cadmium filter were made by using calculated multigroup transport fluxes and adjoint functions for the perturbed reactor containing a cadmium cover, and were applied by rewriting expression (3) as follows:

$$\frac{\Delta K}{NVK} = - CI_{eff} \left[\frac{\sum_i I^{calc}_{eff,i} \varphi(u)_i \varphi^*(u)_i}{I^{calc}_{eff}} \right] \tag{5}$$

The bracketed term in equation (5) is the calculated multigroup importance correction

factor for the measured reactivity coefficients. The calculated flux and adjoint per unit lethargy $\varphi(u)_i$ and $\varphi^*(u)_i$ are normalized to 1 at the main gold resonance energy of 4.9 electron volts; the resulting correction factors for the tungsten isotopes measured varied from 1.0 to 1.1. Therefore, the use of expression (4) in conjunction with the individual isotopic correction factors is satisfactory for the reactor used in the present experiments.

The reactivity effects due to inelastic scattering by the sample (refs. 9 and 10) are given by

$$\frac{\Delta K}{NVK} = \frac{\int_0^\infty \sigma(E \rightarrow E')\varphi(E)[\varphi^*(E') - \varphi^*(E)]dE'}{F_{tot}} \tag{6}$$

where $\sigma(E \rightarrow E')$ is the inelastic-scattering transfer cross section from E to E', and $\varphi^*(E') - \varphi^*(E)$ is the change in adjoint function from E to E', which for a thermal reactor is positive and opposite in sign to the resonance capture reactivity. The inelastic-scattering reactivity coefficient of equation (6) is difficult to calculate accurately because the transfer cross sections are generally unavailable. However, the reactivity coefficient may be measured for a highly inelastic-scattering but low-capturing material such as lead. When using this experimental inelastic-scattering reactivity coefficient for lead, the coefficients for other heavy elements may be estimated analytically. This calculation was made by using the evaporation model (ref. 11) and the known total inelastic cross sections of the elements involved. The resulting correction to the data is generally small and unimportant except for the largest samples of low-capture cross-section material.

EXPERIMENT

The reactivity measurements were made in the NASA ZPR-1, which is an unreflected uranyl fluoride - water solution reactor. The reactor vessel, shown in figure 1, is a cylinder that is 30.5 centimeters in diameter and 76.2 centimeters in height. It is supported equidistantly from the walls of the reactor room by a large steel platform that provides access to the reactor core. The fuel solution consisted of 93.3 percent enriched uranium 235 as uranyl fluoride in water and was normally stored in the horizontal tanks below the reactor. The fuel solution concentration used was about 7 percent by weight uranyl fluoride with a hydrogen to uranium 235 atom ratio of about 500. Criticality was achieved by pumping the fuel solution into the reactor vessel in small increments. The reactor was controlled entirely by variation of the solution height. A cadmium safety

rod poised above the reactor solution provided a shutdown mechanism only.

Reactivity measurements were made by suspending the samples at the center of the reactor vessel in the wire sample holder shown in figure 2. The samples were separated from the fuel solution by a 0.89-millimeter-wall cadmium cover contained in a thin-wall Lucite cylinder. Of the several cylinders used, the maximum size was 6.3 centimeters in diameter and 1.6 centimeters in height. The critical solution height was about 46 centimeters for the fuel concentration used; solution heights were measured with a remotely operated micrometer lead screw connected to an electric probe. Changes in solution height can be measured to ±0.2 mil, which corresponds to ±0.02 cent of reactivity for this core.

The reactivity of a sample at the center of the core was determined as the difference between critical heights ΔH for the following two reactor conditions: A critical height was first determined with the sample holder and empty cadmium cover in the reactor and then with the sample in the cadmium cover. After several experiments were performed with different samples, the critical height with the sample holder and empty cadmium cover was redetermined to assure that reference reactor conditions were maintained. A reference critical solution height of 45.720 centimeters at a reference solution temperature of 21.1° C was maintained.

Corrections for gradual changes in critical height that are caused by small fuel-solution temperature changes during sample measurements were made by using an experimentally determined temperature coefficient of reactivity of 0.1145 centimeter ΔH per °C. Other second-order differences in critical heights that were not accounted for by fuel temperature changes were caused by gradual evaporation of water from the fuel solution. Evaporation was minimized by enclosing the reactor with a plastic cover, which enabled the humidity to be controlled. The reactivity correction for residual evaporation varied with reactor room relative humidity but was typically 0.0013 centimeter ΔH per hour. The reference fuel concentration was maintained by the occasional addition of water to the fuel solution.

Period measurements. - The proportionality between changes in solution height ΔH and reactivity was obtained from measurements of stable reactor periods and the in-hour relation. The period measurements were made by using two counting channels employing standard boron fluoride filled proportional counters surrounded with paraffin. The reactor was returned to a just critical condition for 10 minutes or longer following each period determination.

The increments of reactor height ΔH and corresponding reactivities are shown in figure 3. The data indicate a linear variation of reactivity with ΔH over the range measured. The maximum value of ΔH, 235 mils, was near the practical limit for obtaining good period data. The largest value of ΔH observed for any of the samples measured was 150 mils. Since the curve is linear and only relative reactivities are of

interest in the present measurements, the measured values of ΔH need not be converted to reactivity units in order to determine effective resonance integrals.

Reactor flux and adjoint spectrum. - Inasmuch as I_{eff} is defined for a $1/E$ slowing-down spectrum, it is desirable that measurements be made in an approximate $1/E$ flux spectrum or in a device which has this energy response. Measurements of resonance integrals have generally been made in portions of moderators that are remote from fuel elements, in which a $1/E$ spectrum is assured. The present measurements were made with a uranyl fluoride - water fuel solution surrounding the sample. The fuel solution was, however, quite dilute with a hydrogen to uranium 235 atom ratio of 500, so that the neutron energy spectrum approximated a $1/E$ slowing-down spectrum. Time-of-flight spectral measurements (refs. 12 and 13) of neutron flux in boron-water solutions and uranium 235 - water mixtures of comparable absorptivity indicate an apparent $1/E$ spectrum to exist. However, these measurements extend only to energies of about 20 electron volts and deviations from $1/E$ are difficult to discern.

Flux and adjoint calculations were made for the ZPR-1 reactor to evaluate deviations from $1/E$ with precision. The central flux and adjoint inside a cadmium cover, shown in figure 4, indicate that neither the flux nor the adjoint is constant with lethargy. However, in the important region where most captures occur, between 1 and 1000 electron volts, the fluxes and adjoints vary slowly. The calculations shown in figure 4 were made with GAM II (ref. 14) generated cross sections and a one-dimensional transport code using the P_1S_8 approximation. The calculations were for a reactor with hydrogen to uranium 235 ratio of 500 containing a spherical cadmium cover with a 1.86-centimeter inside radius and a 0.089-centimeter wall thickness. The reduction in adjoint flux at lethargies greater than 12 was caused by the cadmium. Adjoint fluxes above a lethargy of 8 as computed by diffusion theory were significantly lower than the P_1S_8 transport solutions shown in figure 4. The reduction in adjoint flux at high lethargy values was also dependent on the radius of the cadmium cover.

There were small dips within the group fluxes caused by uranium 235 and cadmium resonances that are not shown in figure 4 but are delineated by the finer group structure that was used in reference 15. These flux dips do not correspond in energy with any of the resonances of gold and tungsten samples measured, with the exception of a small cadmium resonance at 18.5 electron volts. The cadmium resonance could be important in shielding the 18.8-electron-volt resonance of tungsten 186. However, the calculated transmission of the cadmium cover indicated the effect of this resonance on the tungsten measurements was less than 3 percent. Wing interferences for uranium 235 resonances were computed to be negligible in reference 16. Several measurements of the effects of different cadmium cover sizes on measured values of ΔH for a given gold sample were made to obtain additional information on the effects of adjoint flux variation and to intercalibrate results for various sized samples. These data are shown in figure 5 in which

the reactivity ΔH for a 2.54-centimeter-diameter by 0.25-centimeter-thick gold disk is plotted against the critical height of the reactor with the different cadmium boxes. Each cover had a 0.89-millimeter-thick cadmium wall. The decreasing values of ΔH for the gold sample with increasing cadmium cover size are attributed in part to a decrease in central-core-region importance with increased cadmium cover size. This decrease in importance is thought to be somewhat greater than the data show because the reactor height is significantly greater for the larger cover data and values of ΔH per unit of reactivity increase approximately as the cube of the reactor height (ref. 17).

Measurements were also made of the change in the shape of the curve of figure 5 for gold samples of other sizes. The effect of gold sample size, however, was small and proved to be beyond the resolution of the measurements. The measurements shown in figure 5 therefore provide a direct means for comparing reactivity data measured with different cadmium cover sizes for all the samples measured.

Relative γ-ray activity measurements. - Radioactive isotopes are formed from neutron capture by gold, tungsten 186, and tungsten 184. Relative neutron capture rates, as indicated by counting the 0.41 MeV γ-ray for a range of sample sizes, were measured for gold to supplement the reactivity data. The gold activation data were used to establish the reference reactivity coefficients.

The gold foils were irradiated at a reactor power of approximately 10 watts in the same sample holder as was used for the reactivity measurements. Reactor power was monitored by a 0.0127-centimeter-thick gold foil placed in a fixed position outside the core. The foils were counted 10 centimeters from a 7.6- by 7.6-centimeter sodium iodide crystal. The use of conventional scintillation counting and interchanging of the order of counting for all samples in a short time interval minimized equipment drift errors. The γ-ray attenuation corrections were minimized by making the thick samples from stacks of thin ones and individually counting the foils.

RESULTS AND DISCUSSION

Reactivity Coefficient Data for Gold

The measured reactivities for gold samples 2.54 centimeters in diameter and 0.0127 to 1.9 centimeters thick were converted into reactivity coefficients in units of mils change in critical core height per 10^{24} sample atoms. The relative γ-ray activity data for thin samples ranging in thickness from 0.152 to 10^{-6} centimeter must be normalized with the reactivity data in the region of common thicknesses. These data are then used to determine the constant of proportionality of equation (4) which relates the reactivity coefficients to effective resonance integrals. The dilute resonance integral for

gold was used as a standard with which to compare thick gold data and the tungsten isotopic data.

Differences between the reactivity and the activity data for gold that are dependent on sample size must be considered prior to normalizing these data. As mentioned before, the observed negative reactivity data for absorptive samples included an inelastic scattering effect that is opposite in sign to the resonance capture effect. Therefore, the observed negative reactivity data must be made more negative by correcting for the inelastic reactivity effect prior to normalization with the activity data. A second difference between the activity and reactivity gold data results from the adjoint weighting of the capture rate as a function of neutron energy, which is required for the reactivity data only. The corrections for this effect are calculated to be less than 3 percent.

The inelastic scattering effect for gold is significant and was determined relative to the reactivity coefficient of 14.7 mils per 10^{24} atoms that was measured for lead. Differences between lead and gold were estimated by using published total inelastic cross sections (ref. 1) in conjunction with the evaporation model (ref. 11) to obtain the energy distribution of the inelastically scattered neutrons. In these calculations, the flux and adjoint energy variations shown in figure 4 were used. The resulting gold sample reactivity coefficient due to inelastic scattering was evaluated to be 40 mils per 10^{24} atoms. The inelastic scattering corrections were made to the gold reactivity data which are then directly comparable to the gold activity data.

The corrected reactivity coefficients and the relative γ-ray activity data are presented in figure 6 where they are plotted against a generalized geometric parameter, the sample surface-to-mass ratio to the 1/2 power $(S/M)^{1/2}$. The activity data were normalized to a best-fit curve through the reactivity data in the region of common sample size. The uncertainties in the data, given by the bars, were determined from the standard deviation of sample activities, sample mass uncertainty, and reproducibility of reactivity measurements.

Effective Resonance Integrals for Gold

Effective resonance integrals were calculated for gold in order to assess the validity of gold as a standard for measuring effective resonance integrals and to determine the constant of proportionality of equation (4) which relates the reactivity coefficients to effective integrals. These calculations were made by using the computer codes ZUT and TUZ (ref. 18) and the published resonance parameters (ref. 19). The calculations are normalized to the thin sample data for gold as shown by the solid curve in figure 6. The calculated effective resonance integrals and the reactivity coefficients are in very good agreement over the entire range of $(S/M)^{1/2}$. A small mismatch occurs for the largest samples, which could be caused by lack of precision in the correction for the inelastic

scattering effect. The magnitude of the inelastic scattering effect is indicated by the dashed curve in figure 6 in which the positive reactivity effect of inelastic scattering is included. The calculated reactivity coefficient for the larger samples (smaller $(S/M)^{1/2}$) is reduced approximately 10 percent by inelastic scattering.

The data of figure 6 provide the constant of proportionality for equation (4) which relates the reactivity coefficients in units of mils increase in reactor solution height per 10^{24} atoms to a dilute value of I_{eff} for gold of 1575 barns as

$$C = 10.0 \pm 0.5 \text{ mils}/(10^{24} \text{ atoms}) \times (b)$$

The general agreement of calculated and measured values of I_{eff} over a large range of $(S/M)^{1/2}$ attests to the validity of the calculational procedures used and to the relative precision and completeness of the known resonance parameters. It is interesting to note that the major contributions to I_{eff} for the large sample sizes were not from the prominent resonances but from the capture cross sections below the first resonance and from the unresolved high-energy cross sections that are not well known. Calculations for several gold sample sizes were made in which broad energy groups were used to illustrate the relative contributions to I_{eff} of various energy regions. The results of the group calculations of I_{eff} and for the flux and adjoint weighted values of I_{eff} are shown in table I.

In the first group, extending from the standard cadmium cutoff energy of 0.5 electron volt to $3/7\ E_o$ for the main gold resonance, the value of I_{eff} is determined by numerically integrating the capture cross section (ref. 20). In this integration the following relation is used:

$$I_{eff} = \int_{0.5 \text{ eV}}^{3.7\ E_o} P_o \sigma_c(E) \frac{dE}{E} \tag{7}$$

where the escape probabilities P_o used are for an infinite slab of equivalent $(S/M)^{1/2}$ as tabulated in reference 21. The unresolved s-wave integrals were obtained from a Nordheim calculation which cuts off at 12.8 kiloelectron volts. Contributions for higher angular momentum neutrons were numerically integrated with no selfshielding by using gold capture cross sections of reference 1.

The calculation of $I_{eff}\varphi(u)\varphi^*(u)$ and also $I_{eff}\varphi(u)$ applicable to a direct capture rate measurement was made with the group split shown in figure 4 and was then combined into the groups shown in table I. The importance factor $\varphi(u)\varphi^*(u)$ for the first group accounts for captures below 0.5 electron volt as well as the lowered flux and adjoint in the group. A comparison of the total of the I_{eff} column and the total of flux-weighted or flux- and adjoint-weighted I_{eff} columns for the various sample sizes $(S/M)^{1/2}$ at the bottom of

TABLE I. - IMPORTANCE-WEIGHTED EFFECTIVE RESONANCE INTEGRAL OF GOLD

Neutron energy interval, eV	Calculated flux and calculated adjoint flux, $\varphi(u)\varphi^*(u)$	Calculated flux, $\varphi(u)$	Sample size, $(S/M)^{1/2}$, $cm/g^{1/2}$											
			321.9			3.219			1.018			0.3219		
			Effective resonance integral, I_{eff}	Flux- and adjoint-weighted resonance integral, $I_{eff}\varphi(u)\varphi^*(u)$	Flux-weighted resonance integral, $I_{eff}\varphi(u)$	Effective resonance integral, I_{eff}	Flux- and adjoint-weighted resonance integral, $I_{eff}\varphi(u)\varphi^*(u)$	Flux-weighted resonance integral, $I_{eff}\varphi(u)$	Effective resonance integral, I_{eff}	Flux- and adjoint-weighted resonance integral, $I_{eff}\varphi(u)\varphi^*(u)$	Flux-weighted resonance integral, $I_{eff}\varphi(u)$	Effective resonance integral, I_{eff}	Flux- and adjoint-weighted resonance integral, $I_{eff}\varphi(u)\varphi^*(u)$	Flux-weighted resonance integral, $I_{eff}\varphi(u)$
0.50 to 2.11	0.70	0.85	36.2	[a]25.3	[a]30.8	34.7	[a]24.3	[a]29.5	28.2	[a]19.7	[a]24.0	11.2	[a]7.8	[a]9.5
2.11 to 7	1.00	1.00	1461.4	1461.4	1461.4	243.5	243.5	243.5	68.1	68.1	68.1	12.9	12.9	12.9
7 to 100	1.08	1.06	39.8	43.0	42.2	17.6	19.0	18.7	6.6	7.1	7.0	2.2	2.4	2.3
100 to 200	1.15	1.12	11.1	12.8	12.4	6.9	7.9	7.7	3.2	3.7	3.6	1.2	1.4	1.3
200 to 400	1.15	1.12	8.8	10.1	9.9	6.2	7.1	6.9	3.1	3.6	3.5	1.3	1.5	1.5
400 to 600	1.16	1.13	3.9	4.5	4.4	3.0	3.5	3.4	1.8	2.1	2.0	.6	.7	.7
600 to 900	1.16	1.13	3.7	4.3	4.2	3.6	4.2	4.1	2.0	2.3	2.3	.9	1.1	1.0
Unresolved s-wave	1.21	1.18	8.9	10.7	10.5	8.7	10.5	10.3	6.4	7.8	7.6	3.1	3.7	3.7
Higher ℓ	1.90	2.4	1.7	3.2	4.1	1.7	3.2	4.1	1.7	3.2	4.1	1.7	3.2	4.1
Total			1575.5	1575.3	1580.7	325.9	323.2	328.2	121.1	117.6	122.2	35.1	34.7	37.0
Importance correction factor, $I_{eff}\varphi(u)\varphi^*(u)/I_{eff}$				1.00			0.99			0.97			0.99	

[a]The lower energy limit for this calculation is zero.

table I, indicates only small differences because of compensation in the flux weighting of the contributions above and below the main gold resonance at 4.9 electron volts. The large attenuation in the group containing the main gold resonance is noted.

Effective Resonance Integrals for Tungsten 182

The enriched tungsten 182 samples contained about 5 percent of the other tungsten isotopes and the calculated contribution to I_{eff} due to these isotopes is 10 percent or less of the total over the range of sample sizes. Thus, the comparison between calculation and measurement is primarily for the tungsten 182 isotope.

The results for samples enriched in tungsten 182 are shown in figure 7(a). Values of I_{eff} are obtained from reactivity measurements for 5.72-centimeter-diameter disks of tungsten trioxide with the exception of the thickest sample which is a metallic cylinder 2.5 centimeters in diameter by 2.5 centimeters long. For the oxide samples, values of $(S/M)^{1/2}$ and the reactivity coefficients were computed for the contained tungsten. A possible reactivity effect due to neutron capture or inelastic scattering by oxygen in the absence of resonance capture by tungsten was investigated by measuring the reactivity of a large sample of carbon, which, within the experimental uncertainty, was zero. Because of the similarities in carbon and oxygen cross sections, it was concluded that the oxygen also has a negligible effect on reactivity.

The importance correction factor in equation (5) for tungsten 182 was calculated to be 1.02 to 1.03 for the range of sample sizes used. The correction is greater than 1 due to larger contributions above the 4.9-electron volt reference energy of gold. The experimental reactivity coefficients for tungsten 182 were accordingly reduced by an average of 2.5 percent. An additive correction of 40 mils per 10^{24} atoms for inelastic scattering was also made to these data. The uncertainty in the data shown in figure 7(a) was determined from the uncertainty in the reactivity coefficient measurement plus an estimated uncertainty of 10 mils per 10^{24} atoms for the inelastic scattering correction, which corresponds to 1 barn on the I_{eff} scale.

The samples contained slightly different isotopic compositions as shown in figure 7(a); however, the isotopic variations negligibly affected the calculated results. The effects of neutron scattering by oxygen were included in the calculation of the oxide samples but had negligible effect for samples of $(S/M)^{1/2}$ greater than about 1.

The resonance parameters used in the calculations for the isotopes of tungsten are shown in table II. The parameters for the first resonance for each isotope were obtained

TABLE II. - RESONANCE PARAMETERS FOR TUNGSTEN ISOTOPES

Energy, eV	Neutron width, Γ_n, eV	Capture width, Γ_γ, eV	Spin factor
Tungsten 182			
4.17	0.00148	0.054	1
21.1	.039	.058	
114.7	.290	.061	
214.0	.003	.058	
250.0	1.1	.055	
282.0	.0029		
343.0	.006		
378.0	.13		
430.0	.28		
486.0	.5		
580.0	.3		
658.0	.16		
762.0	.069		
922.0	.4		
951.0	2.2		
1010.0	.49		
1100.0	1.6		
1170.0	.48		
Tungsten 183			
7.65	0.0018	0.077	3/4
27.13	.042		
40.6	.0017		
46.08	.154		
47.8	.115		
66.0	.016		
100.8	.100		
103.9	.012		1/4
137.7	.0045		3/4
144.5	.100		1/4
155.0	.400		1/4
157.1	.067		3/4
174.1	.130		3/4
192.4	.035		3/4
235.5	.022		1/4
240.4	.059		1/4
243.4	.019		3/4
259.2	.066		
280.5	.260		
297.6	.044		
323.0	.200		
337.0	.035		
348.0	.170		
362.0	.039		
391.6	.043		
418.7	.057		
460.9	.086		1/4

Energy, eV	Neutron width, Γ_n, eV	Capture width, Γ_γ, eV	Spin factor
Tungsten 184			
102.1	0.0027	0.047	1
184.7	1.12		
244.0	.0023		
311.0	.085		
424.0	.04		
684.0	.68		
787.0	.06		
802.0	1.6		
961.0	1.6		
1000.0	.14		
1090.0	3.4		
1140.0	.34		
1270.0	1.2		
1410.0	2.7		
1430.0	.25		
1520.0	1.3		
1650.0	.5		
1790.0	1.4		
2050.0	2.2		
2090.0	5.3		
Tungsten 186			
18.83	0.318	0.044	1
171.5	.027	.060	
197.6	.0004	.055	
218.0	.53	.055	
288.0	.026	.060	
407.0	.075	.055	
512.0	.056		
543.0	.50		
666.0	.75		
732.0	2.2		
835.0	.017		
968.0	1.1		
1080.0	.65		
1130.0	.45		
1190.0	.77		
1420.0	.25		
1510.0	1.2		
1800.0	.10		
1940.0	.55		
2040.0	.40		
2120.0	.11		

from Harvey (ref. 4). Parameters for the higher energy resonances were obtained from references 3 and 6. Capture cross sections below the first resonance were obtained from reference 20. The calculation and measurement of I_{eff} for the tungsten 182 samples are in general agreement but with the calculations lying about 5 percent below the measurements. This agreement is well within the reported errors in the resonance parameters and capture cross sections.

Effective Resonance Integrals for Tungsten 183

Sufficient material enriched in tungsten 183 was available to prepare three samples. The isotopic enrichment was not as high as for the enriched tungsten 182, and 20 percent of the calculated I_{eff} was contributed by the nontungsten 183 isotopes in the samples. The results for these samples are shown in figure 7(b). The two thin samples were tungsten trioxide disks, 5.72 centimeters in diameter, and the thick sample was a metallic cylinder, approximately 2.5 centimeters long and 2.5 centimeters in diameter. The experimental data contains a correction of 40 mils per 10^{24} atoms for inelastic scattering and a net importance correction factor of 1.05.

The calculated curves for the tungsten 183 samples lie 5 percent below the oxide data, whereas the metallic sample data point is on the calculated curve.

Effective Resonance Integrals for Tungsten 184

The calculated contribution of tungsten 184 to I_{eff} of the samples measured was only 25 percent, even though the samples were 94 percent enriched in relatively nonabsorptive tungsten 184. Effective resonance integrals obtained from samples enriched in the tungsten 184 isotope are shown in figure 7(c). Sample sizes and composition were similar to those of the other isotopes, and the data contains the 40-mils-per-10^{24}-atoms inelastic-scattering correction and a net importance factor correction of 1.06. Calculation and experiment are in agreement within the experimental uncertainty. For the metallic cylinder sample with a $(S/M)^{1/2}$ ratio of 0.4, the accuracy of the measured I_{eff} depends on the precision of the relatively large inelastic scattering correction. The large uncertainty shown in figure 7(c) includes a 25-percent uncertainty in the inelastic scattering correction. The calculated curve is seen to lie slightly below the experimental data points for the oxide samples.

Effective Resonance Integrals for Tungsten 186

The samples used contained 97 percent tungsten 186 and 2 percent tungsten 184 with 1 percent of the other isotopes. The calculated contribution to I_{eff} due to nontungsten 186 isotopes accounted for 5 to 7 percent of the total integral. The relative contributions of various energy groups to I_{eff} for pure tungsten 186 are presented in table III, which also indicates the flux- and adjoint-weighted values of I_{eff}. The dominance of the group containing the 18.8-electron-volt resonance is noted.

A comparison of the calculations and measurements for the enriched samples is shown in figure 7(d). The tungsten 186 reactivity data are for tungsten trioxide disks, 5.72 centimeters in diameter, and a metallic cylinder, approximately 2.5 centimeters in diameter by 2.5 centimeters long. The data contain a correction of 40 mils per 10^{24} atoms for inelastic scattering. For tungsten 186, the importance correction factor of equation (5) is obtained from the results shown in table III. For thin samples, the calculated importance weighted factor $I_{eff}\varphi(u)\varphi^*(u)$ is larger than I_{eff} because the dominant contribution to I_{eff} is at 18.8 electron volts where the importance factor is larger than at the gold resonance reference energy of 4.9 electron volts. For very thick samples, a significant part of the total contribution to I_{eff} lies below 4.9 electron volts, so that the net correction factor is 1. For tungsten 186, therefore, a relatively large contribution to I_{eff} below the 18.8-electron-volt group and an unusually small contribution above this group results in a net variation of importance correction with lump size. This variation of net importance correction factor with sample size was not observed for the other isotopes.

The data shown in figure 7(d) indicate the calculations to be about 10 percent above the measurements for the oxide samples and 20 percent above the measurement for the metal sample. The difference between experiment and calculation is less than reported previously (ref. 22) because of recent changes in the measured resonance parameters for the 18.8-electron-volt resonance (ref. 4) and in the capture cross sections below this resonance (ref. 20). The cross sections of tungsten 186 are well known with the exception of the value of Γ_γ for the 18.8-electron-volt resonance, so that a detailed comparison of the calculations and experimental results in figure 10 may indicate probable values of Γ_γ.

The reported error in the cross sections of reference 20 below the 18.8-electron-volt resonance is 3 percent. The value of Γ_n for the tungsten 186 resonance (ref. 4) is 0.318±0.003 electron volt; however, Γ_γ is reported as 0.041±0.009 electron volt from area analysis and 0.055±0.006 electron volt from shape analysis. On the other hand, the value of Γ_γ for the 18.8-electron-volt resonance cannot exceed 0.044±0.002 electron volt in order to calculate the recently measured thermal cross section (ref. 20) using the resonance parameters. This value of Γ_γ was used in the calculations shown

TABLE III. - IMPORTANCE-WEIGHTED EFFECTIVE RESONANCE INTEGRAL OF TUNGSTEN 186

Neutron energy level, eV	Calculated flux and calculated adjoint flux, $\varphi(u)\varphi^*(u)$	Sample size, $(S/M)^{1/2}$, $cm/g^{1/2}$									
		321.9		32.19		3.219		1.018		0.3219	
		Effective resonance integral, I_{eff}	Flux- and adjoint-weighted resonance integral, $I_{eff}\varphi(u)\varphi^*(u)$	Effective resonance integral, I_{eff}	Flux- and adjoint-weighted resonance integral, $I_{eff}\varphi(u)\varphi^*(u)$	Effective resonance integral, I_{eff}	Flux- and adjoint-weighted resonance integral, $I_{eff}\varphi(u)\varphi^*(u)$	Effective resonance integral, I_{eff}	Flux- and adjoint-weighted resonance integral, $I_{eff}\varphi(u)\varphi^*(u)$	Effective resonance integral, I_{eff}	Flux- and adjoint-weighted resonance integral, $I_{eff}\varphi(u)\varphi^*(u)$
0.50 to 8	0.88	17.2	[a]15.3	17.2	[a]15.3	17.1	[a]15.2	15.7	[a]13.94	10.6	[a]9.45
8 to 80	1.06	446.1	473.0	389.3	413.0	94.0	99.7	33.0	35.0	9.4	9.98
80 to 180	1.10	2.6	2.86	2.6	2.86	1.6	1.76	.5	.55	.2	.22
180 to 250	1.13	4.3	4.86	4.1	4.63	2.1	2.37	.8	.90	.4	.45
250 to 450	1.13	1.7	1.92	1.6	1.81	1.2	1.35	.5	.57	.2	.23
450 to 700	1.17	1.4	1.63	1.4	1.64	.9	1.05	.4	.47	.2	.23
700 to 1200	1.17	1.2	1.40	1.1	1.29	.5	.58	.4	.47	.2	.23
1200 to 2200	1.19	.3	.36	.3	.36	.3	.36	.2	.24	.1	.12
Unresolved s-wave	1.20	.5	.60	.5	.60	.5	.60	.4	.48	.2	.24
Higher ℓ	2.20	.2	.44	.2	.44	.2	.44	.2	.44	.2	.44
Total		475.5	502.0	418.3	442.0	118.4	123.3	52.1	53.0	21.7	21.59
Importance correction factor, $I_{eff}\varphi(u)\varphi^*(u)/I_{eff}$			1.06		1.06		1.04		1.02		1.00

[a]The lower energy limit for this calculation is zero.

in figure 7(d) which lie above the experimental results.

For the highly scattering tungsten 186 resonance at 18.8 electron volts, the calculational method using the ZUT code (ref. 18) is believed to be inadequate. Cohen (ref. 23) investigated the limitations of the ZUT-TUZ calculational procedure which requires the assumption of flat-source distribution in the absorber sample in order to compute collision probabilities. By relaxing this flat-source assumption for the 18.8-electron-volt resonance, Cohen found that detailed transport calculations result in a 10 to 20 percent reduction in I_{eff} for $(S/M)^{1/2}$ from 1.0 to about 0.1 relative to the flat-source calculation. This error corresponds quite closely to the differences in the Nordheim calculations and experiment shown in figure 7(d). Therefore a value of Γ_γ of 0.044 electron volt is actually in excellent agreement with the experiments when the results of the study of reference 23 are applied.

The experimental errors shown in figure 7(d) do not include a gold standardization error common to all the isotopes measured. This gold standardization error consists of a 5 percent error in the constant C of equation (4), a $2\frac{1}{2}$ percent error in the gold resonance integral, and an error of approximately 1 percent due to uncertainties in the importance correction factors. The root-mean-square error in the experimental tungsten 186 integrals is estimated as 8 percent for values of $(S/M)^{1/2}$ less than 2. Based on this net uncertainty and the calculations of Cohen (ref. 23) a value of Γ_γ of 0.044±0.004 electron volt for the 18.8-electron-volt resonance is recommended.

Effective Resonance Integrals for Natural Tungsten

Experimental effective resonance integrals for metallic samples of natural tungsten are shown in figure 7(e). The samples are small cylinders 2.5 centimeters long with diameters as large as 2.5 centimeters for values of $(S/M)^{1/2}$ below 0.45, and are 3.8 by 5.1 centimeter rectangles up to 1 centimeter thick for the larger values of $(S/M)^{1/2}$. The error bars on the data points represent the uncertainty in the reactivity measurement plus 1 barn, corresponding to a 25 percent uncertainty in the correction of 40 mils per 10^{24} atoms for inelastic scattering. A calculated importance correction factor of 1.05 is used that results from the preponderance of captures above the gold reference at 4.9 electron volts. Both corrections are estimated to be independent of sample size.

The calculated curve in figure 7(e) overestimates the experimental data for the thicker samples by 10 to 20 percent. In the present calculations, a slab sample of natural tungsten was considered to consist of noninteracting slabs of the individual isotopes; that is, contributions from each resonance of each isotope were computed separately and individually summed so that any resonance overlap effects are not included. Therefore, a comparison of calculations for the summed isotopes and experiments for

TABLE IV. - ESTIMATE OF RESONANCE OVERLAP EFFECTS

Sample size $(S/M)^{1/2}$, $cm/g^{1/2}$	Calculated error, percent				
	Tungsten	Tungsten 182	Tungsten 183	Tungsten 186	Tungsten error from isotopes
1.2	0	-4	-5	5	~-1
.8	0	-3	-5	7	~0
.5	12	-3	-3	9	~1
.3	25	0	0	17	~6

natural tungsten serves as a test of the degree of interaction between the isotopic resonances in natural tungsten. This comparison is shown in table IV for four sample sizes of natural tungsten. The first column shows the percent calculated overestimates of the measured natural tungsten effective resonance integrals. The next three columns show the corresponding percentages for the individual absorptive tungsten isotopes as measured. The last column is the resulting calculated overestimate in the natural tungsten calculation based on the individual contribution of the important isotopes. Comparison of the first and last columns shows that the natural tungsten data exhibit an interaction between the various resonances that results in greater selfshielding.

The differences between experiment and overestimated calculations for natural tungsten can be explained by the partial overlap of some of the larger isotopic resonances that is not considered in the Nordheim calculation. A recently developed calculational method (ref. 24) that considers resonance overlap was not used here. This method should provide better calculational agreement with the natural tungsten data. Resonance overlap would be expected to become more important for large samples as indicated by the results in figure 7(e). A recent Monte Carlo calculation (ref. 25) indicated a significant reduction in effective integrals of large samples of natural tungsten because of resonance overlap.

CONCLUSIONS

Effective resonance integrals were determined relative to gold for natural tungsten and samples highly enriched in the individual isotopes of tungsten. The data are in good agreement with the Nordheim calculation for tungsten 182, 183, and 184; however, this calculational method, utilizing recent resonance parameters, overestimated values of the effective resonance integrals for tungsten 186 and thick samples of natural tungsten.

For tungsten 186, the use of a resonance capture width of 0.044±0.004 electron volt for the 18.8-electron-volt resonance brings the Nordheim calculation and experiment into much better agreement. The remaining disagreement for tungsten 186 and thick samples of natural tungsten appeared to be explained by recent calculations of the error in the ZUT-TUZ results caused by the flat source and isolated resonance approximations.

APPENDIX - SYMBOLS

C	constant relating I_{eff} and reactivity coefficient, mils/(10^{24} atoms)(b)
E, E'	neutron energy, eV
E_{Cd}	cadmium cutoff energy, eV
E_o	resonance energy
F_{tot}	integrated total fission rate in reactor
ΔH	change in reactor height, mil
I_{eff}	effective resonance integral, b
$\Delta K/K$	reactivity
M	mass, g
N	sample atom density, atoms/cm^3
P_o	escape probabilities
r	spatial variable, cm
S	surface, cm^2
u	lethargy
V	sample volume, cm^3
Γ_n	resonance neutron width, eV
Γ_γ	resonance capture width, eV
$\varphi(E)$	neutron flux per unit energy, n/(cm^2)(sec)(eV)
$\varphi(u)$	neutron flux per unit lethargy
φ_o	total unperturbed neutron flux, n/(cm^2)(sec)
φ^*	adjoint flux
σ_c	microscopic capture cross section, b

Subscript:

i	energy group

REFERENCES

1. Hughes, Donald J.; and Schwartz, Robert B.: Neutron Cross Sections. Rep. No. BNL-325 (2nd ed.), Brookhaven National Lab., July 1, 1958.

2. Hughes, D. J.; Magurno, B. A.; and Brussel, M. K.: Neutron Cross Sections. Rep. No. BNL-325 (2nd ed.) (Suppl. 1), Brookhaven National Lab., Jan. 1, 1960.

3. Khan, F. A.; and Harvey, J. A.: Parameters of Neutron Resonances in ^{184}W. Nucl. Sci. Eng., vol. 25, no. 1, May 1966, pp. 31-36.

4. Harvey, J. A.: The Measurement of Neutron Total Cross Sections in the Resonance Energy Region and the Determination of Resonance Absorption. Rep. No. ORNL-P-1885, Oak Ridge National Lab., 1965.

5. Block, R. C.; and Sullivan, J. G.: Multiple Scattering Corrections to Neutron Capture Data. Some Recent Nuclear Cross Section Measurements at ORNL, June 2, 1964 - October 1, 1964, P. H. Stetson. Rep. No. ORNL-TM-954, Oak Ridge National Lab., Sept. 23, 1964, p. 4.

6. Block, R. C.; Hockenbury, R. W.; and Russell, J. E.: The Parameters of the Neutron Resonances in ^{182}W, ^{183}W, ^{184}W, and ^{186}W. Physics Division Annual Progress Report for Period Ending December 31, 1965. Rep. No. ORNL-3924, Oak Ridge National Labs., May 1966, pp. 31-35.

7. Dresner, Lawrence: Resonance Absorption in Nuclear Reactors. Pergamon Press, 1960.

8. Nordheim, L. W.: A New Calculation of Resonance Integrals. Nucl. Sci. Eng., vol. 12, no. 4, Apr. 1962, pp. 457-463.

9. Hurwitz, Henry, Jr.: Note on the Theory of Danger Coefficients. Rep. No. KAPL-98, Knolls Atomic Power Lab., Sept. 18, 1948.

10. Stewart, H. B.; and Storm, M. L.: Reactivity Coefficient Systematics. The Physics of Intermediate Spectrum Reactors. Vol. 3 of Naval Reactor Physics Handbook. J. R. Stehn, ed., AEC, Sept. 1958, pp. 89-91.

11. Weinberg, Alvin M.; and Wigner, Eugene P.: The Physical Theory of Neutron Chain Reactors. University of Chicago Press, 1958.

12. Poole, M. J.: Measurements of Neutron Spectra in Moderators and Reactor Lattices-1. Aqueous Moderators. J. Nucl. Energy, vol. 5, no. 3/4, 1957, pp. 325-341.

13. Young, J. C.; Trimble, G. D.; Houston, D. H.; Heid, P. R.; and Beyster, J. R.: Measurement of Neutron Spectra and Decay Constants in a Water Moderated Multiplying Assembly. Am. Nucl. Soc. Trans., vol. 4, no. 2, Nov. 1961, p. 269.

14. Joanou, G. D.; and Dudek, J. S.: Gam-11.A B_3 Code for the Calculation of Fast-Neutron Spectra and Associated Multigroup Constants. Rep. No. GA-4265, General Atomic Div., General Dynamics Corp., Sept. 16, 1963.

15. Fieno, Daniel: Consistent P1 Analysis of Aqueous Uranium-235 Critical Assemblies. NASA TN D-1102, 1961.

16. Kelber, Charles N.: A Simple Estimate of the Effects of Resonance Interference. Nucl. Sci. Eng., vol. 22, no. 1, May 1965, pp. 120-121.

17. Gwin, R.; Trubey, D. K.; and Weinberg, A. M.: Experimental and Theoretical Studies of Unreflected Aqueous U^{235} Critical Assemblies. Reactor Physics. Vol. 12 of the Proceedings of the Second United Nations International Conference on the Peaceful Uses of Atomic Energy. United Nations, 1958, pp. 529-538.

18. Kuncir, G. F.: A Program For the Calculation of Resonance Integrals. Rep. No. GA-2525, General Atomic Div., General Dynamics Corp., Aug. 28, 1961.

19. Desjardins, J. S.; Rosen, J. L.; Havens, W. W., Jr.; and Rainwater, J.: Slow Neutron Resonance Spectroscopy. II. Ag, Au, Ta. Phys. Rev., vol. 120, no. 6, Dec. 15, 1960, pp. 2214-2226.

20. Friesenhahn, S. J.; Haddad, E.; Fröhner, F. H.; and Lopez, W. M.: The Neutron Capture Cross Section of the Tungsten Isotopes From 0.01 to 10 Electron Volts. Nucl. Sci. Eng. vol. 26, no. 4, Dec. 1966, pp. 487-499.

21. Case, K. M.; deHoffmann, F.; Carlson, B.; Goldstein, M.; and Placzek, G.: Introduction to the Theory of Neutron Diffusion. Vol. 1. Los Alamos Scientific Lab., June 1953, pp. 17-30.

22. Shook, Donald; and Bogart, Donald: Effective Resonance Integrals of Separated Tungsten Isotopes. Am. Nucl. Soc. Trans., vol. 8, no. 1, June 1965, pp. 284-285.

23. Cohen, Sanford C.: An Improved Treatment of Scattering Resonances in Slab Geometry. Nucl. Sci. Eng., vol. 27, no. 1, Jan. 1967, pp. 133-135.

24. Stevens, C. A.; and Smith, C. V.: Garol - A Computer Program for Evaluating Resonance Absorption Including Resonance Overlap. Rep. No. GA-6637, General Atomic Div., General Dynamics Corp., Aug. 24, 1965.

25. Westfall, Robert M.: Resonance Overlap in Natural Tungsten. Am. Nucl. Soc. Trans., vol. 9, no. 2, Nov. 1966, pp. 504-505.

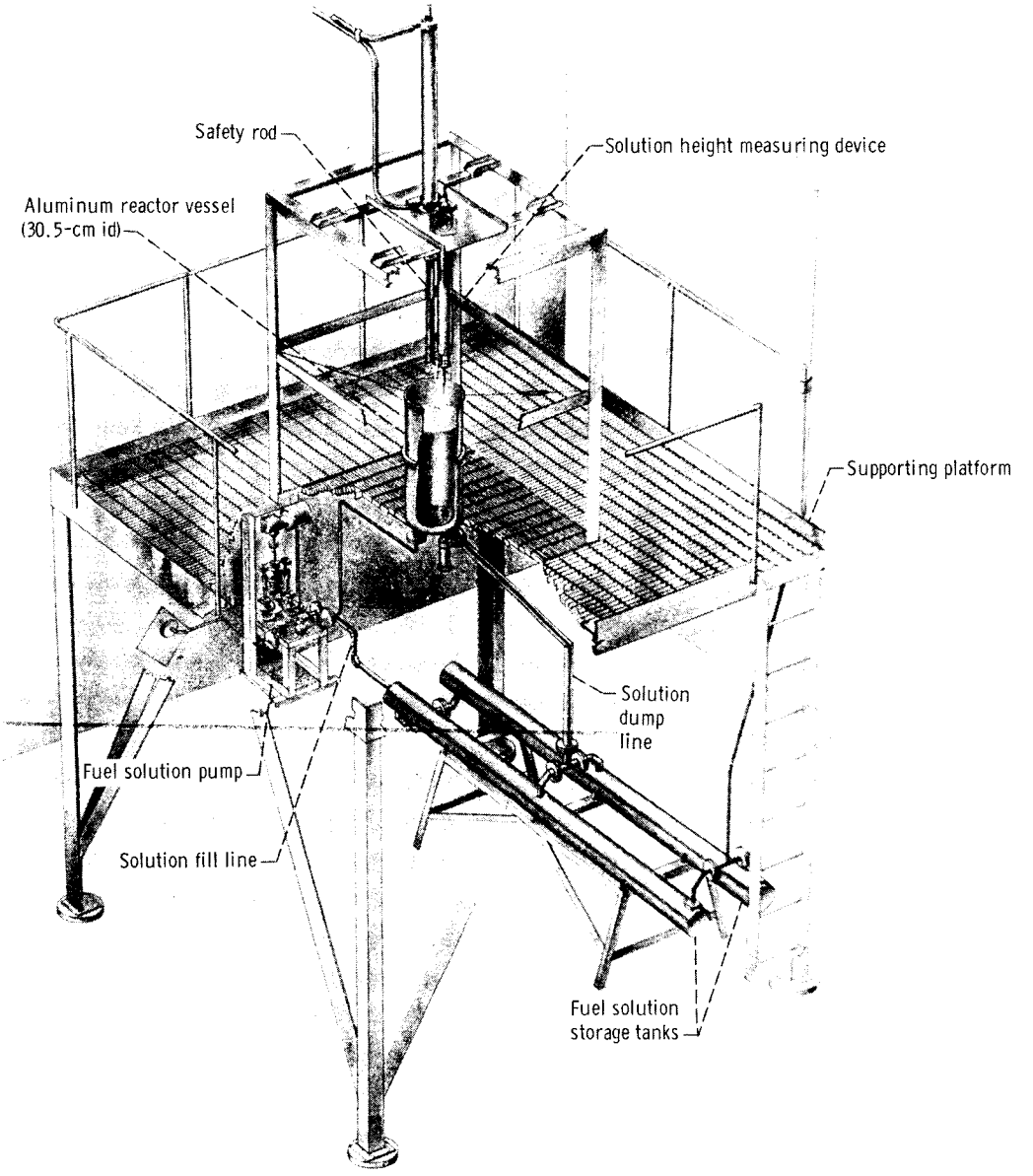

Figure 1. - Uranyl flouride - water solution reactor (NASA ZPR-I).

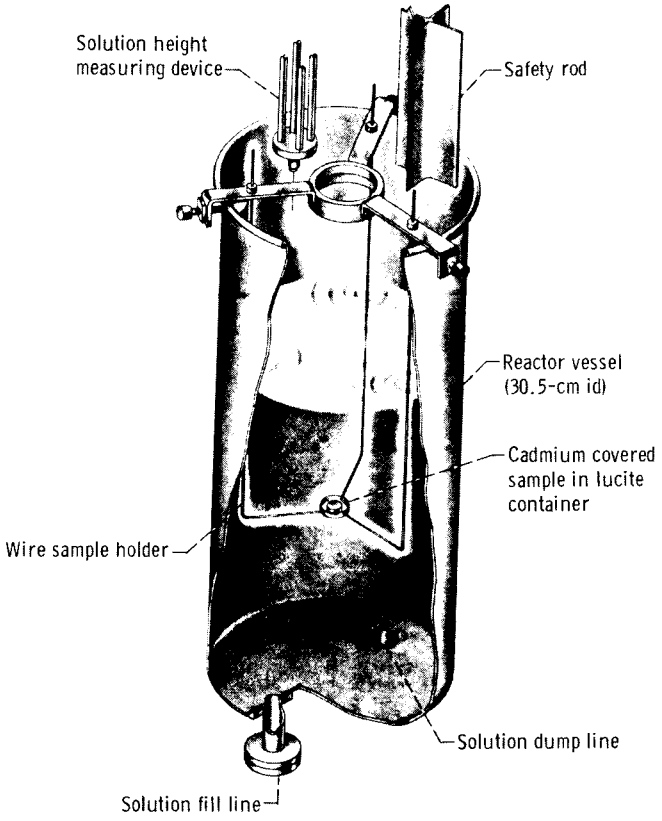

Figure 2. - Samples in reactor vessel.

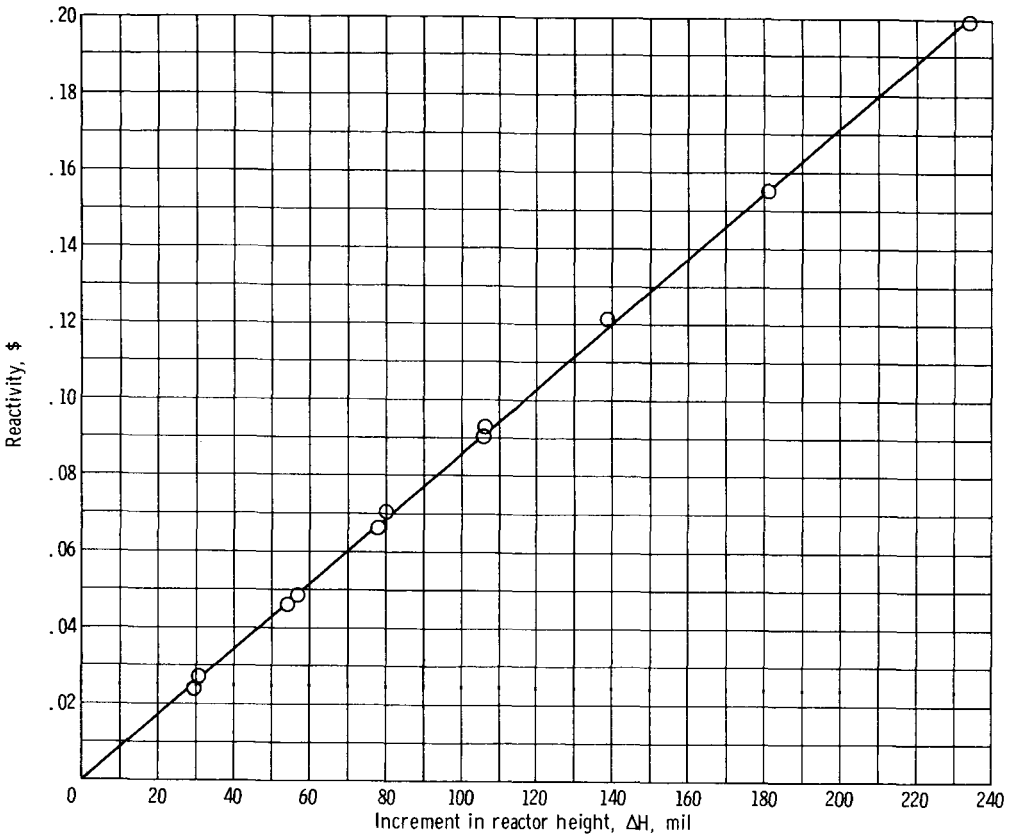

Figure 3. - In-hour data for solution reactor. Reactor critical height, 45.72 centimeters; solution temperature, 21.1° C.

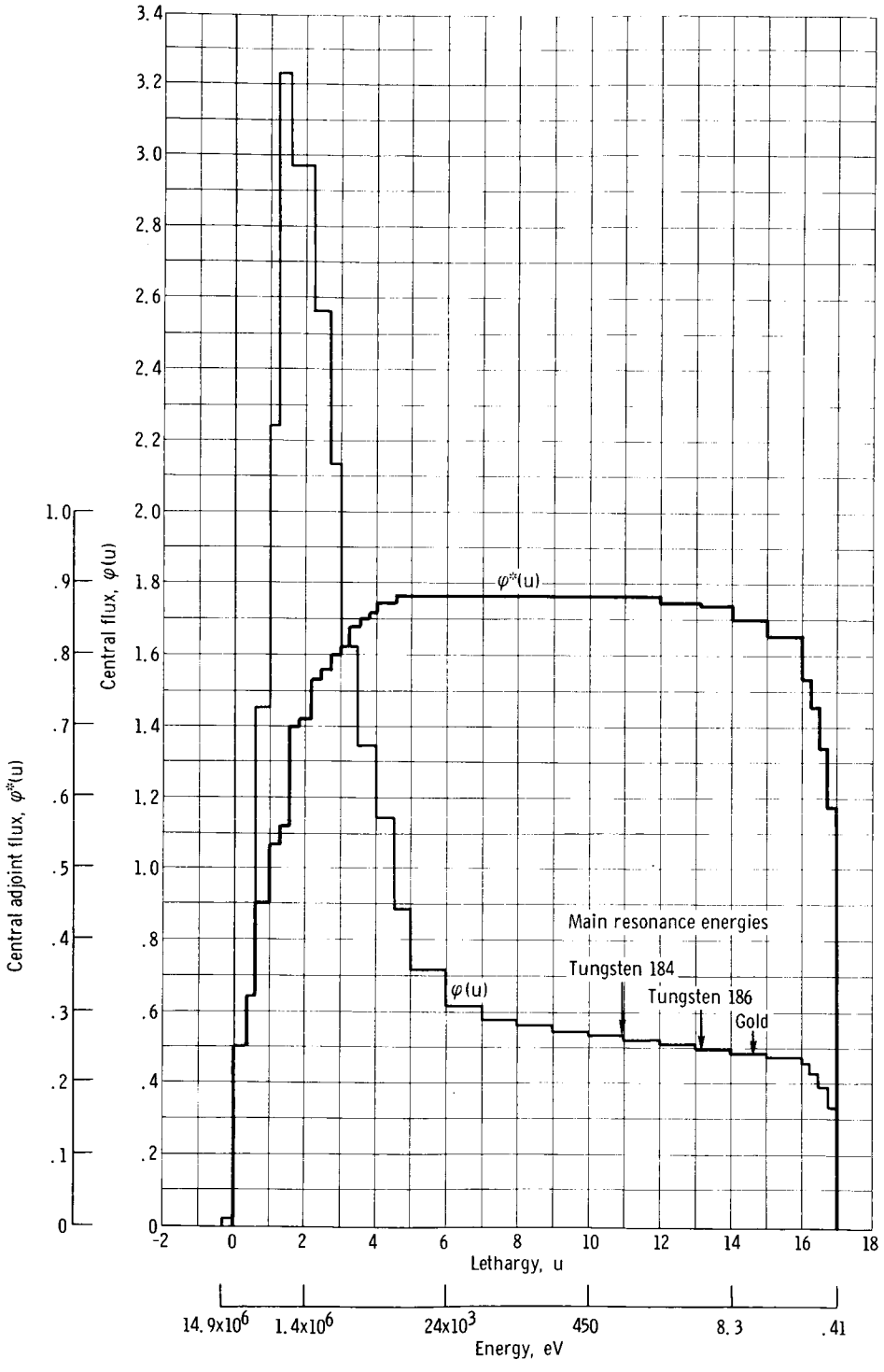

Figure 4. - NASA reactor ZPR-1, central flux and central adjoint flux inside cadmium cover.

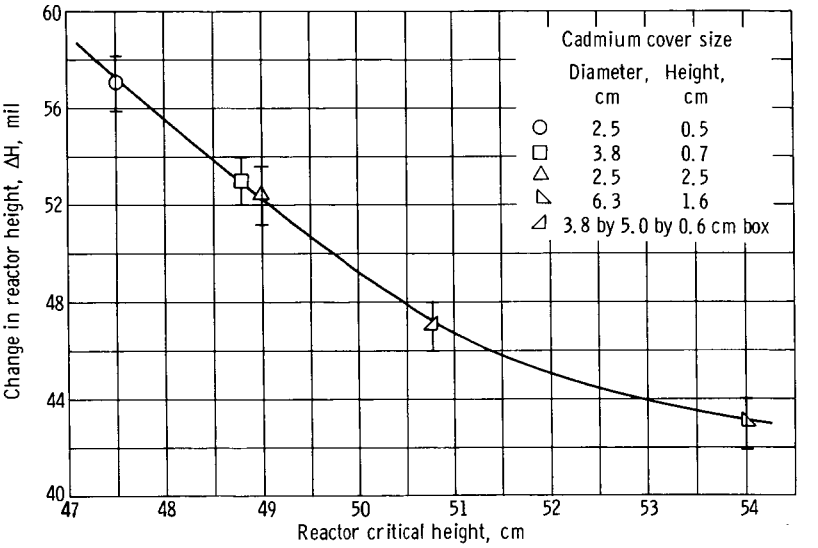

Figure 5. - Variation of reactor height with cadmium cover size for a gold sample.

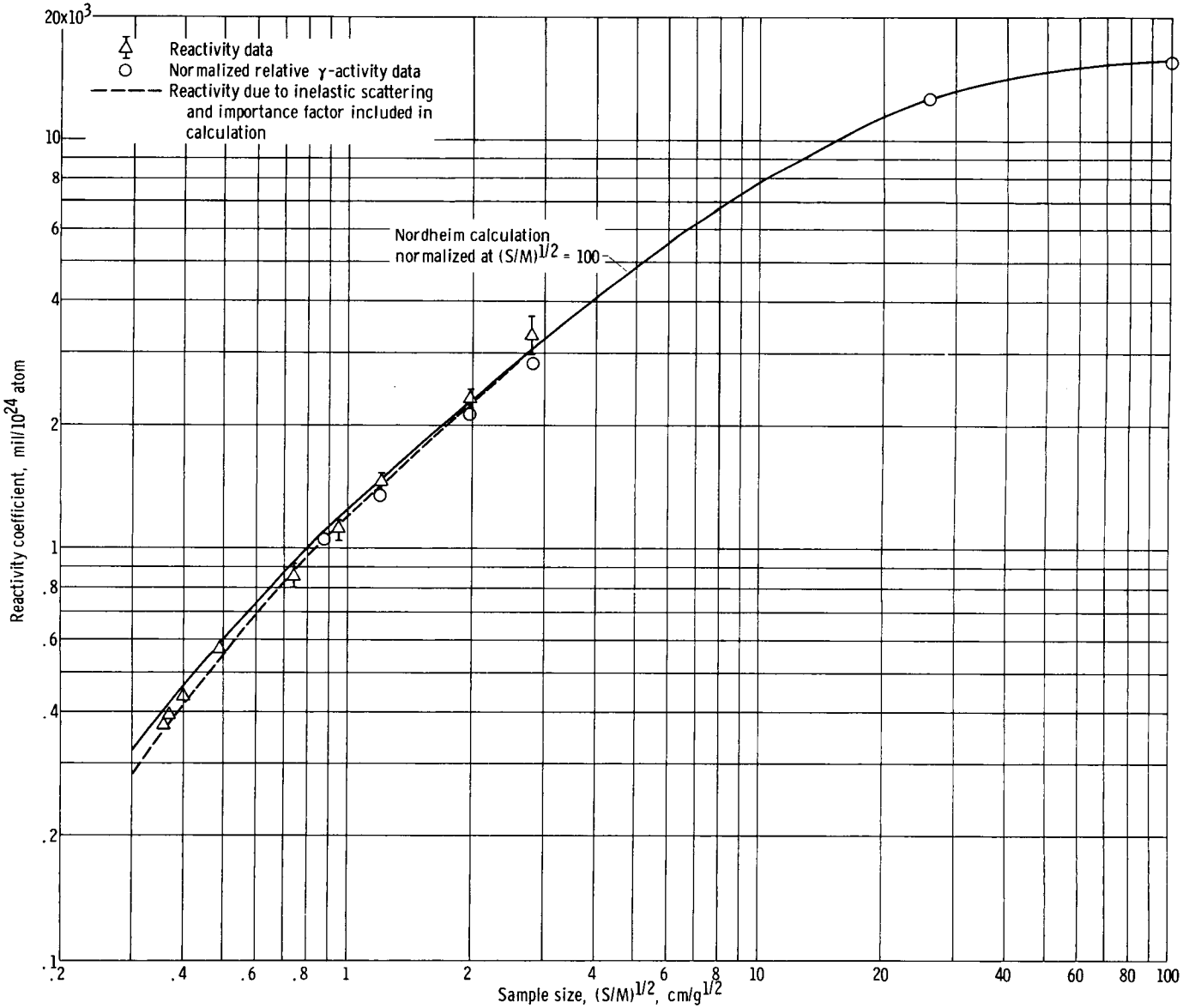

Figure 6. - Gold reactivity coefficients.

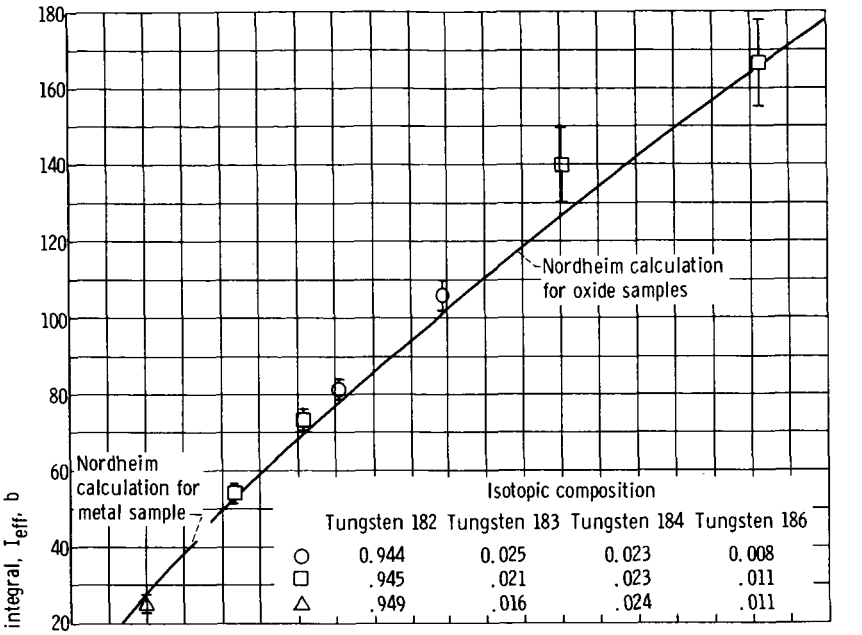

(a) Tungsten 182.

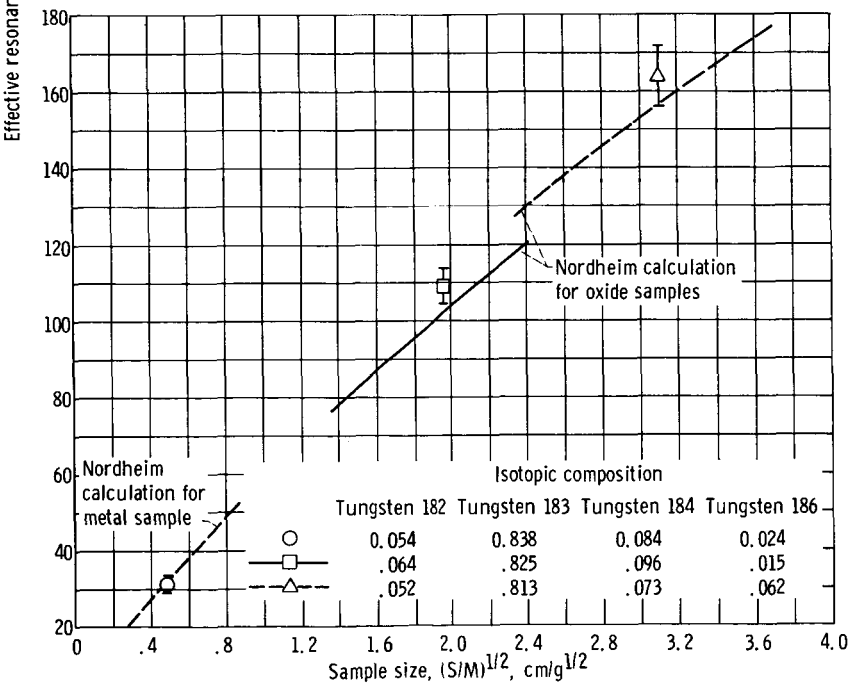

(b) Tungsten 183.

Figure 7. - Measurements of tungsten isotopes and natural tungsten.

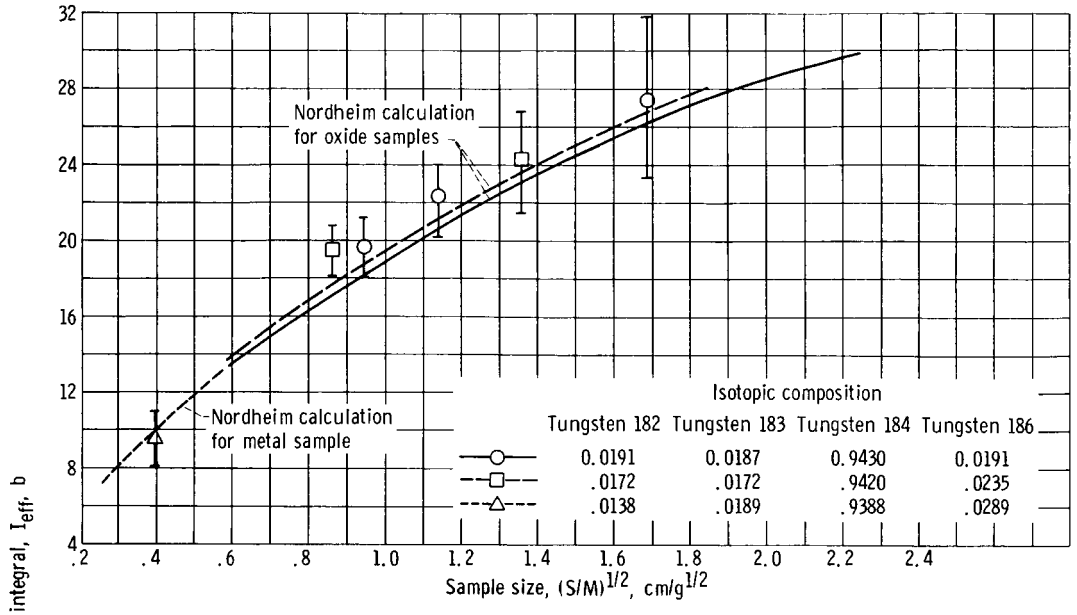

(c) Tungsten 184.

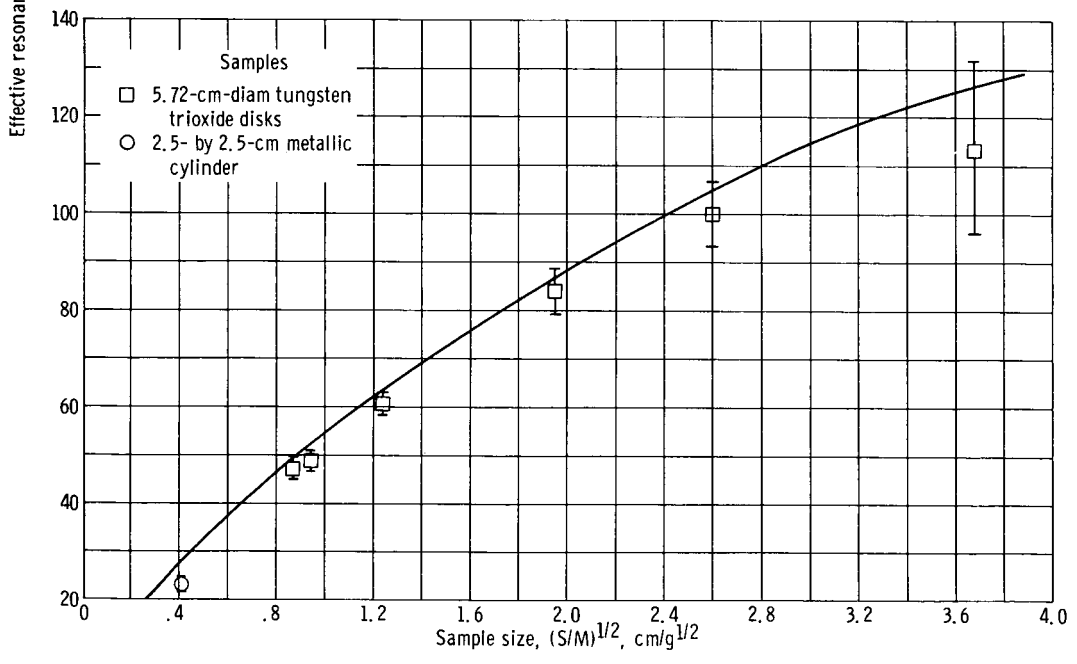

(d) Tungsten 186. Isotopic composition: tungsten 182, 0.004; tungsten 183, 0.008; tungsten 184, 0.021; tungsten 186, 0.972.

Figure 7. - Continued.

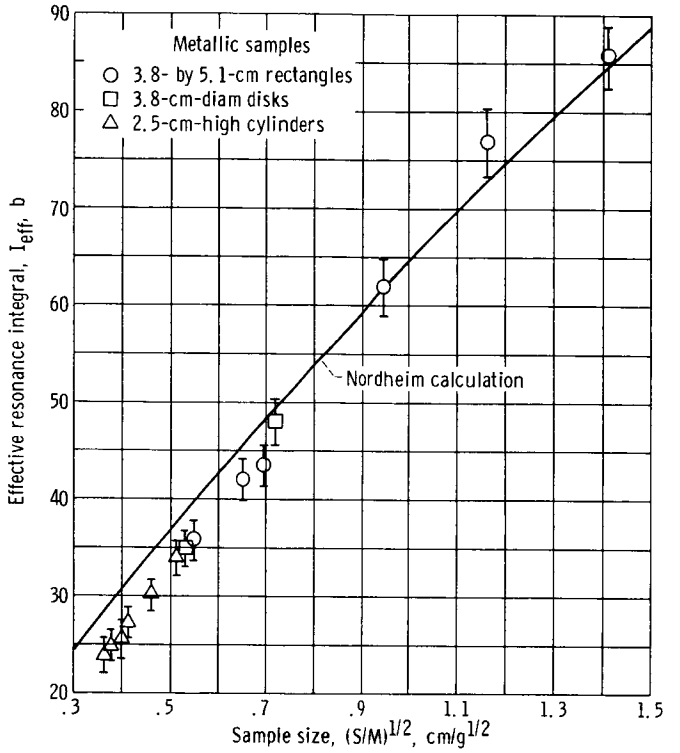

(e) Natural tungsten.

Figure 7. - Concluded.